DANISH METEOROLOGICAL INSTITUTE

SCIENTIFIC REPORT

02-11

Unfolding of Radio Occultation Multipath Behavior Using Phase Models

Kent B. Lauritsen and Martin S. Lohmann

COPENHAGEN 2002

ISSN 0905-3263
ISSN 1399-1949 (online)
ISBN 87-7478-463-3

DMI Scientific Report No. 02-11

Unfolding of Radio Occultation Multipath Behavior Using Phase Models

Kent B. Lauritsen and Martin S. Lohmann

Danish Meteorological Institute, 2100 Copenhagen, Denmark

18 November 2002

Abstract

We have analyzed radio occultation simulations containing various types of multipath behavior. The simulations are performed for global atmospheric fields containing strong refractivity gradients which give rise to multipath behavior. In the case where the medium and the satellite orbits are spherically symmetric the multipath behavior can be unfolded by a Fourier transform of the measured signal where the derivative of the transformed phase at a given frequency is related to the time where that signal frequency occurs. However, small deviations from circular orbits may imply that the multipath behavior cannot be completely unfolded due to the fact that a given instantaneous frequency may occur at more than one time instant. In order to resolve the multipath behavior for realistic satellite orbits, we employ the idea of modifying the measured signal by a model before carrying out a Fourier transform. For certain models, which depend on the measured phase of the simulated signal, we find that multipath behavior can be successfully unfolded. Even very strong multipath behavior, leading to critical refraction, can in some cases also be handled. The combined effect of applying a model and a Fourier transform can be viewed as a specific type of a canonical transform.

1 Introduction

In the present paper we will investigate multipath (MP) behavior in simulated radio occultation data. Recently, the method of performing a canonical transform to the

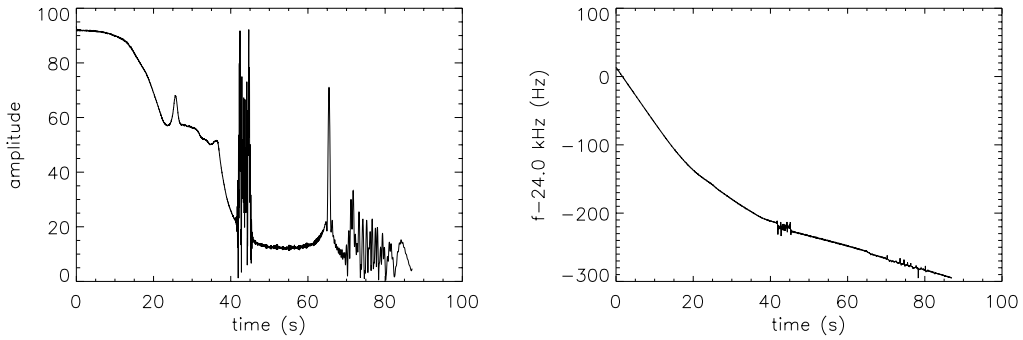

Figure 1: Simulated example with a wave optics propagator showing i) amplitude of a radio signal at the LEO orbit (left), and ii) the Doppler frequency shift (right). One observes strong focusing resulting in multipath behavior with 3 interfering rays appearing around the time 42-46 seconds.

impact parameter representation was introduced in order to unfold multipath behavior in radio occultation measurements [1]. Another recently introduced method consists in Fourier transforming the measured field directly [2]. The canonical transform method can also be applied directly to the measured field and when the satellite orbit degenerates to a circle this canonical transform reduces to a Fourier transform of the measured signal [3]. Here, we will focus on Fourier transforming the measured field for realistic satellite orbits and study whether it is possible to extract the multiple ray structure by applying various phase models.

The simulations we have analyzed have been generated by a wave optics propagator using the multiple phase screen method together with a forward propagation from the last screen to the low-Earth orbit (LEO) satellite [4]. We have used global atmospheric fields obtained from the ECMWF center. In Fig. 1 we show an example of the calculated phase and amplitude containing multipath behavior for a global atmospheric field. The geometry of the radio occultation system is chosen such that the x-axis coincides with the initial propagation direction of the radio waves. The origin of the coordinate system is located in the center of curvature of the occultation point. The simulated field is a solution $u(\mathbf{r}) = A(\mathbf{r})\exp(i\phi(\mathbf{r}))$ to the Helmholtz equation. The signal measured along the LEO trajectory is denoted $u(t)$ and we will also refer to this trajectory as a time direction. The impact parameter for a ray is denoted p and the bending angle ϵ, cf. Fig. 2.

The wavelengths of the GPS radio waves are much smaller than typical atmospheric variations so one expects that geometrical optics can be used to describe the propagation of the wave field [5]. In Fig. 3 is schematically shown the propagation of rays from the GPS satellite towards the LEO satellite in phase space. Initially,

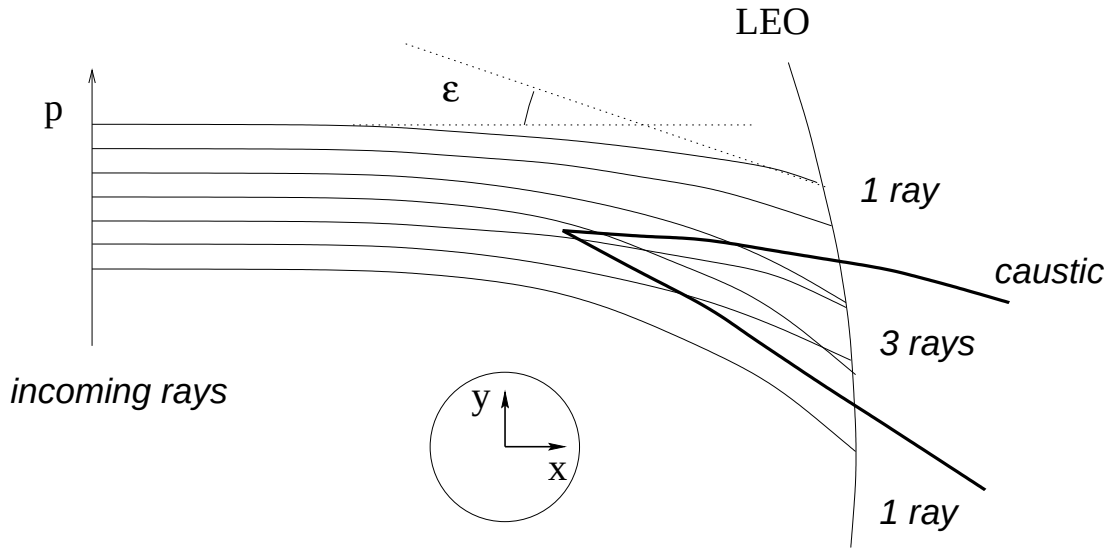

Figure 2: Multipath example: water vapor layers in the lower troposphere give rise to the formation of a caustic (in the example it is a so-called cusp caustic) which surrounds a region with 3 rays passing through any point, implying that 3 rays are arriving at the same time instant at the LEO orbit.

the impact parameter coordinate corresponds to the y coordinate whereas along the LEO orbit the impact parameter is approximately proportional to the associated canonical momentum η.

2 Fourier Transform Method

The field measured at the LEO satellite is $u(t) = A(t)\exp(i\phi(t))$, where the phase term can be written

$$\phi(t) = \int_{t_0}^{t} \omega(t')dt' \,. \tag{1}$$

In the geometrical optics ray picture, the function $\omega(t)$ will be equal to the (total) Doppler shift

$$\omega_D = \vec{k} \cdot \vec{v} \tag{2}$$

in one ray regions whereas in multi-ray regions it will give rise to an $\omega(t)$ that effectively shows the interference structure of multiple rays (cf. Figs. 1–3). Here $\vec{k} = 2\pi/\lambda$ is the wave vector and $\vec{v} = \dot{\vec{r}}$ is the LEO velocity.

Using $\vec{v} = \dot{r}\vec{e}_r + r\Omega\vec{e}_\theta$, with polar coordinate basis vectors $\vec{e}_r = \vec{r}/r$ and $\vec{e}_\theta =$

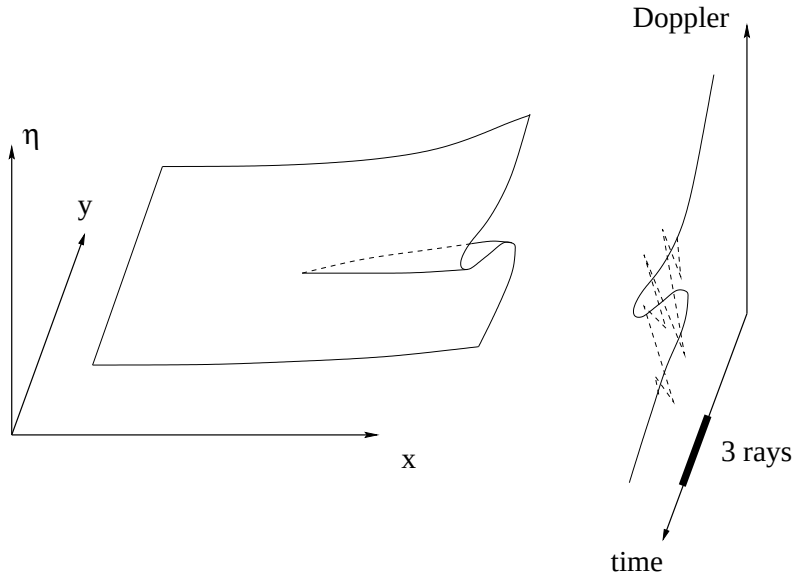

Figure 3: Schematic drawing of phase space showing the ray manifold and its projection onto the Doppler vs. time plot. The propagation direction is x, whereas the canonical momenta associated to y is denoted η. The MP region results in an irregular Doppler signal shown as the dashed line (see also Fig. 1).

$\hat{\vec{r}}/r = \hat{\vec{e}}_\theta$, it follows that the Doppler reads

$$\omega_D = k\dot{r}\sqrt{1-(p/r)^2} + kp\Omega\,, \tag{3}$$

where Ω is the angular velocity related to the satellite-to-satellite angle θ through $\Omega = d\theta/dt$ (note, when the GPS satellite is located at a finite distance r_G an additional term $k\dot{r}_G\sqrt{1-(p/r_G)^2}$ appears on the right hand side).

During an occultation $\Omega(t)$ is practically constant, being of the order of 0.001 s^{-1}, with a variation of the order of 10^{-7} s^{-2}. The $kp\Omega$ term is of the order of 250 krad/s. The other term can be estimated as follows: the distance r to the LEO orbit varies by about 200 meters during an occultation implying that the effect of non-circular orbits results in an effect of the order of 50 rad/s on ω_D. This is comparable to typical MP shifts (the order of MP effects on the Doppler can be estimated to be about 30 rad/s corresponding to a deviation of $\frac{1}{2}\times 10^{-3}$ radians of MP rays).

Upon Fourier transforming $u(t)$ one obtains

$$\tilde{u}(\omega) = F_{t\to\omega}(u(t))(\omega) \equiv B(\omega)\exp(i\psi(\omega))\,, \tag{4}$$

where the phase $\psi(\omega)$ can be written in terms of some function $t(\omega)$ as follows:

$$\psi(\omega) = -\int_{\omega_0}^{\omega} t(\omega')d\omega'\,. \tag{5}$$

The Fourier transform (FT) is defined by the following equation:

$$Ff(\omega) = \widetilde{f}(\omega) = \int e^{-i\omega t} f(t) dt \,, \tag{6}$$

and the inverse Fourier transform reads

$$F^{-1}\widetilde{f}(t) = f(t) = \frac{1}{2\pi} \int e^{i\omega t} \widetilde{f}(\omega) d\omega \,. \tag{7}$$

Note, the choice of the sign convention is due to the fact that t is effectively acting as a space coordinate.

In the limit $k \to 0$, the Fourier transform maps the wave function $u(t)$ to the ω-representation: $\tilde{u}(\omega)$ [6]. In this representation, the function $t(\omega)$ will have a simple, monotonic behavior in one ray regions whereas $t(\omega)$ will show an interference-like structure in multiple ray regions similar to $\omega(t)$. For a non-degenerate stationary phase point, $\phi(t)$ and $\psi(\omega)$ are related by a Legendre transform $\psi(\omega) = \phi(t) - \omega t$, evaluated at the stationary phase point where $\omega = d\phi/dt$ [6]. As a result, the function $t(\omega)$ can be interpreted as the time, t, where the ray with frequency ω appears at the LEO orbit and, using Eq. (3), it follows for circular orbits (and $\Omega = \text{const}$) that ω is proportional to the impact parameter p [2]. In the general case, it has been pointed out that for a spherically symmetric atmosphere the p-representation of the wave function yields a unique ray-structure identification [1].

3 Phase Models

Next, we will investigate the effect of applying a phase term in the Fourier analysis. The purpose of introducing a phase term, $\Delta\phi_m(t)$, is to transform the measured field $u(t)$ in such a way that the Fourier transform will map the signal, not to the ω-representation, but to a pseudo representation which approximates the impact parameter representation.

Generically, the mapping yields a field $u_m(t)$ defined as follows:

$$u_m(t) \equiv A_m(t) \exp(i\phi_m(t)) \,, \tag{8}$$

where the resulting phase model $\phi_m(t)$ reads $\phi_m(t) = \phi(t) + \Delta\phi_m(t)$. Here, we will concentrate on the case where the amplitude is unchanged, i.e., we take $A_m(t) \equiv A(t)$. It should be noted that $\Delta\phi_m(t)$ should not introduce any additional MP-like structure into the signal in order not to destroy the original MP spectrum, i.e., the model $\Delta\phi_m(t)$ should be a slowly varying function.

As the next step, one Fourier transforms the transformed field $u_m(t)$. If one could apply a phase model such that the FT would map the field to the impact

parameter representation then the unfolding of MP would be complete [1]. However, by applying a phase model only, and leaving the amplitude unchanged, we cannot obtain a mapping to the impact parameter representation. Thus, what we seek is a phase model that effectively maps the field to

$$A(t) \exp\left(ik\Omega_0 \int_{t_0}^{t} \tilde{p}(t')dt' \right) ,$$

where $\tilde{p}(t)$ is a quantity which approximately is equal to the impact parameter, and Ω_0 simply sets the scale (e.g., $\Omega_0 = \langle \Omega(t) \rangle$). Expressed in terms of $\Delta\phi_m(t)$, this yields

$$\Delta\phi_m(t) = k\Omega_0 \int_{t_0}^{t} \tilde{p}(t')dt' \, - \phi(t) \, . \tag{9}$$

Note, this $\Delta\phi_m(t)$ depends on the measured field $\phi(t)$.

In the following we will report results for three different phase models. The first is a *linear phase model* defined by the expression [7]

$$\Delta\phi_m(t) = at^2 \, . \tag{10}$$

Here, $d\Delta\phi_m/dt = 2at$, i.e., this model implies that a linear shift is applied to the Doppler $\dot{\phi}$ and it can be interpreted as a rotation of the $\dot{\phi}$-axis. The quantity a is a tunable parameter and by varying it one can investigate how the unfolding of MP behavior is expressed in the (pseudo) ω-representation. In Figs. 4 and 5 we show plots for two different values of a for the MP example shown in Fig. 1. Note, the results are obtained from the numerical derivative of the phase without applying any filtering or smoothing. We observe that by tuning the rotation parameter a we can obtain an unfolding of the MP behavior demonstrated by the nearly constant amplitude of the transformed field. The fact that the amplitude is only approximately constant shows that this representation is only an approximate impact parameter representation.

Next, we will use the Doppler expression (3) [2]. Using this expression, we can obtain two models for our approximate impact parameter $\tilde{p}(t)$:

$$\text{Model 1 :} \qquad \tilde{p}^{(1)}(t) = p^{(0)}(t) \equiv \frac{\dot{\phi}}{k\Omega} \, , \tag{11}$$

$$\text{Model 2 :} \qquad \tilde{p}^{(2)}(t) = p(t) \equiv p^{(0)}(t) + \Delta p(t) \, . \tag{12}$$

Here, $\dot{\phi}$ is the measured Doppler. The function $p(t)$ is the (full) solution of Eq. (3). As noted previously, $\Delta p(t)$ is approximately $10^{-4} - 10^{-3}$ times smaller than $p^{(0)}(t)$. Nevertheless, MP shifts are also about 10^{-4} times smaller than total Doppler shifts so including this term is important.

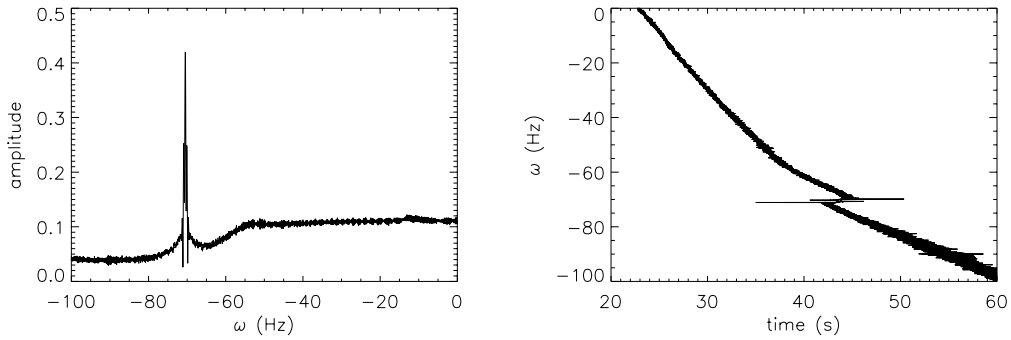

Figure 4: Unfolding of MP behavior using a FT (and no phase model). Left: the amplitude $B(\omega)$ of the FT field; Right: the function $t(\omega)$.

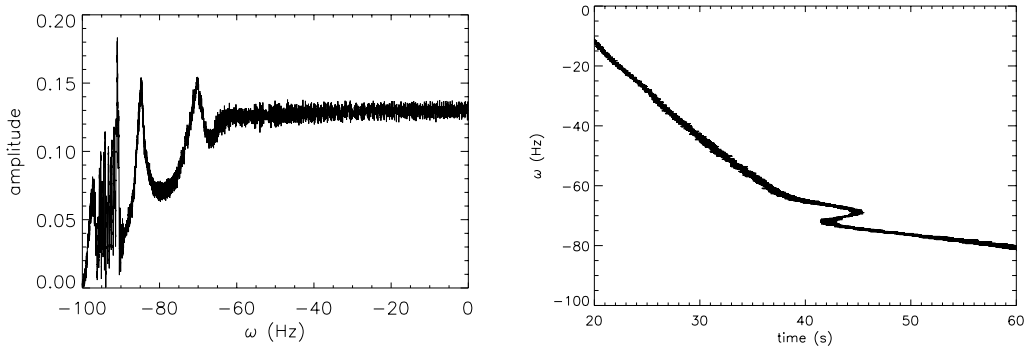

Figure 5: Unfolding of MP behavior using a linear phase model with $a = 0.1$. Left: the amplitude $B(\omega)$ of the FT field; Right: the function $t(\omega)$. Note the nearly constant amplitude over the multipath region signaling that the unfolding has been complete.

Since $\Omega(t)$ is nearly constant it can be expanded around some t_0 to yield $\Delta\phi_m^{(1)} \approx -\int \dot{\phi}\frac{\Omega'(t_0)}{\Omega(t_0)}(t-t_0)\,dt$, thus the phase model 1 approximately corresponds to a linear phase model, cf. (10). Concerning phase model 2, it follows that in single ray regions the quantity $\tilde{p}^{(2)}(t)$ will be identical to the impact parameter, whereas in the MP region we can think of $\tilde{p}^{(2)}(t)$ as a smoothed impact parameter.

In Figs. 6 and 7 we apply phase model 2 in the analysis of simulations based on global atmospheric fields. Figure 6 show the amplitude and derivative of the transformed phase. The almost constant amplitude signals that a very good unfolding of MP has been achieved. Figure 7 show the bending angle as a function of impact parameter for two simulations. Notice the sharp spikes which signal the presence of

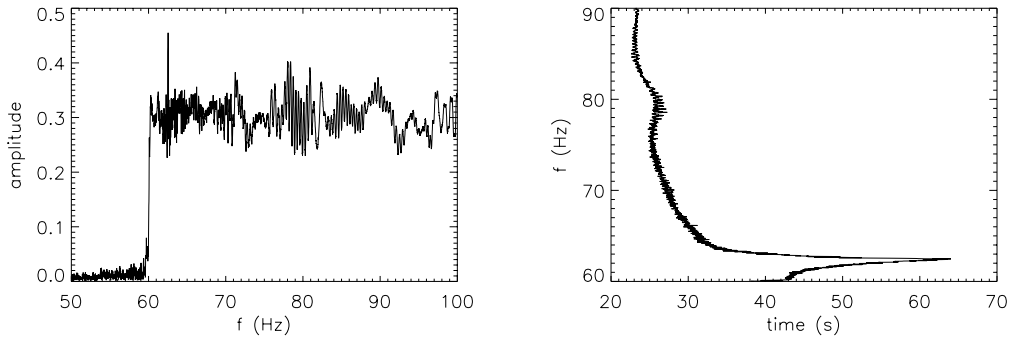

Figure 6: Unfolding of MP behavior using $\tilde{p}^{(2)}(t)$ for a simulation with a global atmospheric field. Left: the amplitude $B(\omega)$ of the FT field; Right: the function $t(\omega)$. Note the nearly constant amplitude over the multipath region signaling that the unfolding has been complete.

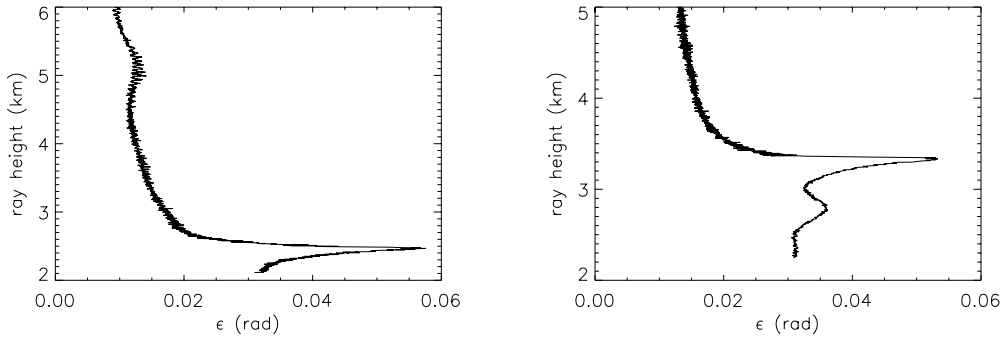

Figure 7: Unfolding of MP behavior using $\tilde{p}^{(2)}(t)$ for the same global field as used in Fig. 6 (left) and for another global atmospheric field (right). The panels show the bending angle $\epsilon(p)$ as a function of ray height (defined as impact parameter minus the local radius of curvature).

critical refraction.

It is possible to formulate the phase model approach as a specific canonical transform. Since $\tilde{p}(t)$ is approximately equal to the impact parameter we expect that the transformed wave function will be able to unfold MP to a high degree. Our results show that this indeed is the case. Furthermore, we observe that model 2 results in a better unfolding of the MP behavior than model 1 in accordance with the fact that model 2 is based on a more precise estimation of the impact parameter.

4 Conclusions

We have carried out a Fourier analysis of radio occultation simulations for various global atmospheric fields. Introducing phase models before performing the Fourier transform, we obtain that multipath behavior can be unfolded for realistic satellite orbits. Specifically, we investigated two models constructed in such a way that they yield an approximate form for the impact parameter. As a result, performing a Fourier transform yields an approximate impact parameter representation of the measured wave field in analogy to the canonical transform method. The resolution of Fourier and canonical transform inversion methods will be limited by atmospheric diffraction which implies that the resolution will be of the order of 30-50 m. Theoretically, however, the resolution limit of geometrical optics based inversion methods can be estimated to be as high as $D\lambda/A$, where D is the distance from the occultation point to the LEO satellite and A the aperture along the LEO orbit.

Acknowledgements

We gratefully acknowledge Michael Gorbunov for providing us with the copy of his wave optics propagator that we used for our simulations. K.B.L. has been supported by EUMETSAT's GRAS Meteorology SAF project. M.S.L. has been supported by ESA's ACE project.

References

[1] (i) Gorbunov, M. E.: Radio-holographic analysis of Microlab-1 radio occultation data in the lower troposphere, J. of Geophys. Res., 107(D12), 10.1029/2001JD000889 (2002); (ii) Gorbunov, M. E.: Canonical transform method for processing GPS radio occultation data in lower troposphere, Radio Science (to appear, 2002)

[2] Jensen, A. S., Lohmann, M. S., Benzon, H.-H., Nielsen, A. S.: Full spectrum inversion method, preprint

[3] Gorbunov, M. E., Lauritsen, K. B.: Canonical transform methods for radio occultation data, preprint

[4] Martin, J.: Simulation of wave propagation in random media: theory and applications, in: Wave propagation in random media (scintillation). eds. V. I. Tatarskii, A. Ishimaru, and V. U. Zavorotny, SPIE - The International Society for Optical Engineering, Bellingham, Washington, USA and Institute of Physics Publishing, Bristol and Philadelphia (1993)

[5] Kravtsov, Y. A., Orlov, Y. I.: Geometrical optics of inhomogeneous media, Springer, Berlin (1990)

[6] Maslov, V. P., Fedoriuk, M. V.: Semi-classical approximations in quantum mechanics, D. Reidel Publishing Company, Dordrecht (1981)

[7] Lauritsen, K. B.: Phase space analysis of multipath, unpublished

DANISH METEOROLOGICAL INSTITUTE

Scientific Reports

Scientific reports from the Danish Meteorological Institute cover a variety of geophysical fields, i.e. meteorology (including climatology), oceanography, subjects on air and sea pollution, geomagnetism, solar-terrestrial physics, and physics of the middle and upper atmosphere.

Reports in the series within the last five years:

No. 97-1
E. Friis Christensen og C. Skøtt: Contributions from the International Science Team. The Ørsted Mission - a pre-launch compendium

No. 97-2
Alix Rasmussen, Sissi Kiilsholm, Jens Havskov Sørensen, Ib Steen Mikkelsen: Analysis of tropospheric ozone measurements in Greenland: Contract No. EV5V-CT93-0318 (DG 12 DTEE):
DMI's contribution to CEC Final Report Arctic Trophospheric Ozone Chemistry ARCTOC

No. 97-3
Peter Thejll: A search for effects of external events on terrestrial atmospheric pressure: cosmic rays

No. 97-4
Peter Thejll: A search for effects of external events on terrestrial atmospheric pressure: sector boundary crossings

No. 97-5
Knud Lassen: Twentieth century retreat of sea-ice in the Greenland Sea

No. 98-1
Niels Woetman Nielsen, Bjarne Amstrup, Jess U. Jørgensen: HIRLAM 2.5 parallel tests at DMI: sensitivity to type of schemes for turbulence, moist processes and advection

No. 98-2
Per Høeg, Georg Bergeton Larsen, Hans-Henrik Benzon, Stig Syndergaard, Mette Dahl Mortensen: The GPSOS project Algorithm functional design and analysis of ionosphere, stratosphere and troposphere observations

No. 98-3
Mette Dahl Mortensen, Per Høeg: Satellite atmosphere profiling retrieval in a nonlinear troposphere Previously entitled: Limitations induced by Multipath

No. 98-4
Mette Dahl Mortensen, Per Høeg: Resolution properties in atmospheric profiling with GPS

No. 98-5
R.S. Gill and M. K. Rosengren: Evaluation of the Radarsat imagery for the operational mapping of sea ice around Greenland in 1997

No. 98-6
R.S. Gill, H.H. Valeur, P. Nielsen and K.Q. Hansen: Using ERS SAR images in the operational mapping of sea ice in the Greenland waters: final report for ESA-ESRIN's: pilot projekt no. PP2.PP2.DK2 and 2nd announcement of opportunity for the exploitation of ERS data projekt No. AO2..DK 102

No. 98-7
Per Høeg et al.: GPS Atmosphere profiling methods and error assessments

No. 98-8
H. Svensmark, N. Woetmann Nielsen and A.M. Sempreviva: Large scale soft and hard turbulent states of the atmosphere

No. 98-9
Philippe Lopez, Eigil Kaas and Annette Guldberg: The full particle-in-cell advection scheme in spherical geometry

No. 98-10
H. Svensmark: Influence of cosmic rays on earth's climate

No. 98-11
Peter Thejll and Henrik Svensmark: Notes on the method of normalized multivariate regression

No. 98-12
K. Lassen: Extent of sea ice in the Greenland Sea 1877-1997: an extension of DMI Scientific Report 97-5

No. 98-13
Niels Larsen, Alberto Adriani and Guido DiDonfrancesco: Microphysical analysis of polar stratospheric clouds observed by lidar at McMurdo, Antarctica

No.98-14
Mette Dahl Mortensen: The back-propagation method for inversion of radio occultation data

No. 98-15
Xiang-Yu Huang: Variational analysis using spatial filters

No. 99-1
Henrik Feddersen: Project on prediction of climate variations on seasonel to interannual timescales (PROVOST) EU contract ENVA4-CT95-0109: DMI contribution to the final report:Statistical analysis and post-processing of uncoupled PROVOST simulations

No. 99-2
Wilhelm May: A time-slice experiment with the ECHAM4 A-GCM at high resolution: the experimental design and the assessment of climate change as compared to a greenhouse gas experiment with ECHAM4/OPYC at low resolution

No. 99-3
Niels Larsen et al.: European stratospheric monitoring stations in the Artic II: CEC Environment and Climate Programme Contract ENV4-CT95-0136. DMI Contributions to the project

No. 99-4
Alexander Baklanov: Parameterisation of the deposition processes and radioactive decay: a review and some preliminary results with the DERMA model

No. 99-5
Mette Dahl Mortensen: Non-linear high resolution inversion of radio occultation data

No. 99-6
Stig Syndergaard: Retrieval analysis and methodologies in atmospheric limb sounding using the GNSS radio occultation technique

No. 99-7
Jun She, Jacob Woge Nielsen: Operational wave forecasts over the Baltic and North Sea

No. 99-8
Henrik Feddersen: Monthly temperature forecasts for Denmark - statistical or dynamical?

No. 99-9
P. Thejll, K. Lassen: Solar forcing of the Northern hemisphere air temperature: new data

No. 99-10
Torben Stockflet Jørgensen, Aksel Walløe Hansen: Comment on "Variation of cosmic ray flux and global coverage - a missing link in solar-climate relationships" by Henrik Svensmark and Eigil Friis-Christensen

No. 99-11
Mette Dahl Meincke: Inversion methods for atmospheric profiling with GPS occultations

No. 99-12
Hans-Henrik Benzon; Laust Olsen; Per Høeg: Simulations of current density measurements with a Faraday Current Meter and a magnetometer

No. 00-01
Per Høeg; G. Leppelmeier: ACE - Atmosphere Climate Experiment

No. 00-02
Per Høeg: FACE-IT: Field-Aligned Current Experiment in the Ionosphere and Thermosphere

No. 00-03
Allan Gross: Surface ozone and tropospheric chemistry with applications to regional air quality modeling. PhD thesis

No. 00-04
Henrik Vedel: Conversion of WGS84 geometric heights to NWP model HIRLAM geopotential heights

No. 00-05
Jérôme Chenevez: Advection experiments with DMI-Hirlam-Tracer

No. 00-06
Niels Larsen: Polar stratospheric clouds microphysical and optical models

No. 00-07
Alix Rasmussen: "Uncertainty of meteorological parameters from DMI-HIRLAM"

No. 00-08
A.L. Morozova: Solar activity and Earth's weather. Effect of the forced atmospheric transparency changes on the troposphere temperature profile studied with atmospheric models

No. 00-09
Niels Larsen, Bjørn M. Knudsen, Michael Gauss, Giovanni Pitari: Effects from high-speed civil traffic aircraft emissions on polar stratospheric clouds

No. 00-10
Søren Andersen: Evaluation of SSM/I sea ice algorithms for use in the SAF on ocean and sea ice, July 2000

No. 00-11
Claus Petersen, Niels Woetmann Nielsen: Diagnosis of visibility in DMI-HIRLAM

No. 00-12
Erik Buch: A monograph on the physical oceanography of the Greenland waters

No. 00-13
M. Steffensen: Stability indices as indicators of lightning and thunder

No. 00-14
Bjarne Amstrup, Kristian S. Mogensen, Xiang-Yu Huang: Use of GPS observations in an optimum interpolation based data assimilation system

No. 00-15
Mads Hvid Nielsen: Dynamisk beskrivelse og hydrografisk klassifikation af den jyske kyststrøm

No. 00-16
Kristian S. Mogensen, Jess U. Jørgensen, Bjarne Amstrup, Xiaohua Yang and Xiang-Yu Huang: Towards an operational implementation of HIRLAM 3D-VAR at DMI

No. 00-17
Sattler, Kai; Huang, Xiang-Yu: Structure function characteristics for 2 meter temperature and relative humidity in different horizontal resolutions

No. 00-18
Niels Larsen, Ib Steen Mikkelsen, Bjørn M. Knudsen m.fl.: In-situ analysis of aerosols and gases in the polar stratosphere. A contribution to THESEO. Environment and climate research programme. Contract no. ENV4-CT97-0523. Final report

No. 00-19
Amstrup, Bjarne: EUCOS observing system experiments with the DMI HIRLAM optimum interpolation analysis and forecasting system

No. 01-01
V.O. Papitashvili, L.I. Gromova, V.A. Popov and O. Rasmussen: Northern polar cap magnetic activity index PCN: Effective area, universal time, seasonal, and solar cycle variations

No. 01-02
M.E. Gorbunov: Radioholographic methods for processing radio occultation data in multipath regions

No. 01-03
Niels Woetmann Nielsen; Claus Petersen: Calculation of wind gusts in DMI-HIRLAM

No. 01-04
Vladimir Penenko; Alexander Baklanov: Methods of sensitivity theory and inverse modeling for estimation of source parameter and risk/vulnerability areas

No. 01-05
Sergej Zilitinkevich; Alexander Baklanov; Jutta Rost; Ann-Sofi Smedman, Vasiliy Lykosov and Pierluigi Calanca: Diagnostic and prognostic equations for the depth of the stably stratified Ekman boundary layer

No. 01-06
Bjarne Amstrup: Impact of ATOVS AMSU-A radiance data in the DMI-HIRLAM 3D-Var analysis and forecasting system

No. 01-07
Sergej Zilitinkevich; Alexander Baklanov: Calculation of the height of stable boundary layers in operational models

No. 01-08
Vibeke Huess: Sea level variations in the North Sea – from tide gauges, altimetry and modelling

No. 01-09
Alexander Baklanov and Alexander Mahura: Atmospheric transport pathways, vulnerability and possible accidental consequences from nuclear risk sites: methodology for probabilistic atmospheric studies

No. 02-01
Bent Hansen Sass and Claus Petersen: Short range atmospheric forecasts using a nudging procedure to combine analyses of cloud and precipitation with a numerical forecast model

No. 02-02
Erik Buch: Present oceanographic conditions in Greenland waters

No. 02-03
Bjørn M. Knudsen, Signe B. Andersen and Allan Gross: Contribution of the Danish Meteorological Institute to the final report of SAMMOA. CEC contract EVK2-1999-00315: Spring-to.-autumn measurements and modelling of ozone and active species

No. 02-04
Nicolai Kliem: Numerical ocean and sea ice modelling: the area around Cape Farewell (Ph.D. thesis)

No. 02-05
Niels Woetmann Nielsen: The structure and dynamics of the atmospheric boundary layer

No. 02-06
Arne Skov Jensen, Hans-Henrik Benzon and Martin S. Lohmann: A new high resolution method for processing radio occultation data

No. 02-07
Per Høeg and Gottfried Kirchengast: ACE+: Atmosphere and Climate Explorer

No. 02-08
Rashpal Gill: SAR surface cover classification using distribution matching

No. 02-09
Kai Sattler, Jun She, Bent Hansen Sass, Leif Laursen, Lars Landberg, Morten Nielsen og Henning S. Christensen: Enhanced description of the wind climate in Denmark for determination of wind resources: final report for 1363/00-0020: Supported by the Danish Energy Authority

No. 02-10
Michael E. Gorbunov and Kent B. Lauritsen: Canonical transform methods for radio occultation data

No. 02-11
Kent B. Lauritsen and Martin S. Lohmann: Unfolding of radio occultation multipath behavior using phase models

No. 02-12
Rashpal Gill: SAR image classification using fuzzy screening method

No. 02-13
Kai Sattler: Precipitation hindcasts of historical flood events

No. 02-14
Tina Christensen: Energetic electron precipitation studied by atmospheric x-rays